energies

MDPI

Article

Torque Ripple Suppression in the 6/4 Variable Flux Reluctance Machine with Open Winding Configuration by Using Harmonic Injection

Xu Liu [1], El Moundher Aouiche [1,*], Abdelaziz Aouiche [2], Yang Cao [1] and Mohammed Echarif Aguida [3]

[1] State Key Laboratory of Reliability and Intelligence of Electrical Equipment, Hebei University of Technology, Tianjin 300130, China
[2] LABGET Laboratory, Department of Electrical Engineering, Faculty of Science and Technology, Echahid Cheikh Larbi Tebessi University, Tebessa 12000, Algeria
[3] School of Electrical and Information Engineering, Tianjin University, Tianjin 300072, China
* Correspondence: 201940000012@stu.hebut.edu.cn

Abstract: High torque ripple can be observed with a 6/4 variable flux reluctance machine (VFRM). In order to minimize the torque ripple in VFRMs, this paper presents a harmonic injection method for 6/4 VFRMs with an open-winding configuration. By analyzing the impact of harmonics on VFRMs, the method involves detecting the third harmonic using a first-order low-pass filter (FLPF). Subsequently, the extracted harmonics are controlled and shifted to counteract the voltage harmonics in both inverters without inducing phase imbalance or overvoltage. With the proposed method, the torque ripple can be significantly reduced by about 50% under load conditions. The effectiveness of the harmonic injection method is validated through a prototype VFRM.

Keywords: VFRM; open-winding; harmonic injection; torque ripple suppression

Citation: Liu, X.; Aouiche, E.M.; Aouiche, A.; Cao, Y.; Aguida, M.E. Torque Ripple Suppression in the 6/4 Variable Flux Reluctance Machine with Open Winding Configuration by Using Harmonic Injection. *Energies* **2024**, *17*, 2753. https://doi.org/10.3390/en17112753

Academic Editors: Loránd Szabó and Marcin Wardach

Received: 26 April 2024
Revised: 18 May 2024
Accepted: 21 May 2024
Published: 4 June 2024

1. Introduction

Emerging as a potential alternative to permanent magnet (PM) machines due to their reduced reliance on rare-earth materials, variable flux reluctance machines (VFRMs) offer unique characteristics [1]. Classified as stator-wound field machines, they feature doubly salient structures and are equipped with both an AC armature winding and a DC field winding [2,3]. A shared DC link is used in conjunction with the open winding to create a closed loop for the DC component (zero-sequence current) [4,5].

Despite the advantages of 6/4 VFRMs, VFRMs face a significant obstacle in the form of torque ripple, primarily due to their unique doubly salient structure and the interaction between the AC armature and DC field windings. This uneven torque output manifests as vibrations, noise, and controllability challenges, particularly detrimental in high-precision applications such as robotics and electric vehicles. Moreover, torque ripple incurs power losses, reduces efficiency, and stresses mechanical components, negatively impacting both reliability and lifespan.

Torque ripple reduction methods are broadly categorized into design-based and control-based techniques. In [6], the researchers explored four different techniques for torque ripple mitigation in VFRMs by adjusting the shape of the rotor. These techniques included multistep shaping techniques, inverse cosine with the third harmonic, inverse cosine, and eccentric circular. Yet, these approaches could lead to a decrease in average torque or elevate the intricacy of manufacturing. In [7], two approaches for determining harmonic current injection were devised. The first relies on 2D finite element analysis (FEA)-derived torque waveforms, offering precision but at the cost of extensive preliminary computations. The second uses an analytical formula, needing only the initial inductance values from FEA, yet both are time-intensive due to the reliance on 2D FEA. Harmonics

are an unavoidable presence in VFRMs with open-winding configuration due to nonlinear loads, switching devices, or imperfect components. Therefore, reducing torque ripple through machine control is often necessary and is the primary emphasis in this paper.

Although reports of harmonic injection control-based torque ripple minimization of VFRMs in academic studies are limited, the methods that can be used are generally categorized into two types: those that rely on feedforward strategies and those that use feedback strategies. For feedforward-based strategies to be effective, an initial step involves creating a detailed model of the torque ripple in the VFRM for accurate prediction. In order to mitigate the predicted torque ripple, the harmonic current has been fine-tuned through complex optimization techniques such as genetic algorithms, neural networks, and Lagrange multipliers [8–10] to determine the harmonic current for torque ripple mitigation. Although these techniques are effective, they come with the drawback of computational heaviness due to their iterative nature.

The strategies based on feedback need a feedback signal that reflects the torque ripple. The torque ripple can cause speed ripples and vibrations in the machine drive, which can function as a feedback signal for mitigating torque ripple. In [11], a piezoelectric sensor was used to measure the vibration signal and regulate the harmonic current to reduce the torque ripple. In [12], based on multiple synchronous rotating frame transformations (MSRFTs), a harmonic estimator was designed to decompose the measured current into the reference frame, and the harmonic currents were controlled by integral feedback controllers in MSRFTs. To accurately observe the harmonic currents in MSRFTs, a closed-loop detection system (CDS) for a high-speed permanent magnet synchronous motor (PMSM) was designed in [13]. The disturbance resistance and harmonic detection capabilities of the system were improved. Furthermore, a feedback calculation strategy was proposed to suppress harmonics. The feedback-based methods have benefits over the feedforward-based methods in terms of being more resilient to machine parameter changes and more computationally efficient.

This paper presents a harmonic injection method based on single synchronous reference frame transformation (SSRFT) for reducing the torque ripple in VFRMs by utilizing a feedback-based strategy that employs current harmonics as the control signal. Unlike previous methods, this method introduces the third harmonic into both the reference voltages instead of the field or armature currents to investigate their impact on output torque. In particular, the harmonic injection method is designed as an extra control loop that reduces the torque ripple by regulating harmonic current references. Within this loop, control over the d axis and q axis of the harmonic current references is independent, and the actual speed is included to obtain accurate harmonics that will be injected to reduce the torque ripple. A couple of FLPFs are used in the SSRFT to obtain the DC component from the harmonic current. The overall harmonic injection method is simple and computationally efficient, as it only uses a couple of proportional-integral (PI) controllers. Experimental validation was performed to confirm the efficacy of this harmonic injection strategy.

2. Mathematical Model of a VFRM

Figure 1a presents the structure of a 6/4 VFRM, where the windings carry both DC and AC currents. Here, the AC part operates as the armature current of the stator and the DC part provides the excitation for the magnetic field. To produce the required DC part, referred to as the zero-sequence current, an open-winding VFRM configuration using two inverters connected through a common DC link is implemented, as shown in Figure 1b.

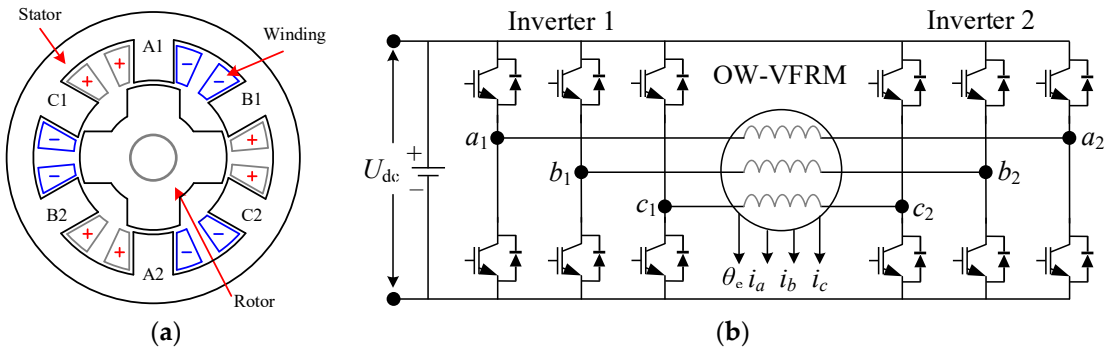

Figure 1. (**a**) Structure of VFRM with zero-sequence current excitation, (**b**) dual inverter with common DC link.

From the perspective of a stationary reference frame, the self-inductance of the armature windings can be formulated as

$$\begin{cases} L_a = L_s + L_\delta \cos(\theta_e) \\ L_b = L_s + L_\delta \cos(\theta_e - 2/3\pi) \\ L_c = L_s + L_\delta \cos(\theta_e + 2/3\pi) \end{cases} \quad (1)$$

where L_δ denotes the fundamental frequency element, while L_s refers to the DC element of the self-inductance. The waveforms and harmonic order of the self-inductances, as derived from FEA modeling, are depicted in Figure 2.

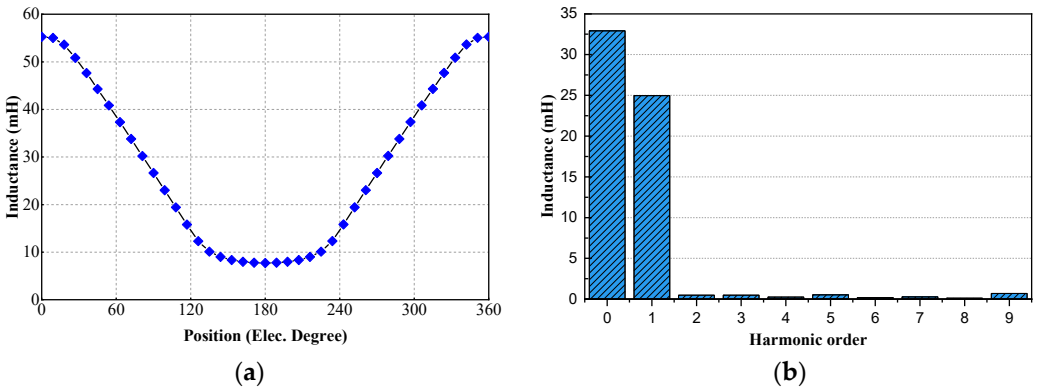

Figure 2. (**a**) Self-inductance waveforms of the 6/4 VFRM (when i_0 = 1 A and ω_e = 400 rpm). (**b**) Harmonic order of self-inductance.

The self-inductance in VFRM primarily comprises a static component and a fundamental frequency harmonic. The amplitude of self-inductance varies concurrently with changes in the DC component, yet the components of the second- and higher-order harmonics remain almost negligible.

Additionally, due to the concentrated winding configuration, the mutual inductance in a VFRM is also practically negligible. Consequently, both mutual inductance and the self-inductance's second- and higher-order harmonic components can be disregarded [1,2]. This simplification applies directly to the armature windings' self-inductances.

As referenced in [14], the voltage Equation (2) of a VFRM includes a third-order variable inductance component.

$$\begin{bmatrix} u_{\mathrm{d}} \\ u_{\mathrm{q}} \\ u_0 \end{bmatrix} = R_s \begin{bmatrix} i_{\mathrm{d}} \\ i_{\mathrm{q}} \\ i_0 \end{bmatrix} + \begin{bmatrix} \frac{L_\delta}{2}\cos 3\theta_{\mathrm{e}} + L_{\mathrm{s}} & -\frac{L_\delta}{2}\sin 3\theta_{\mathrm{e}} & L_\delta \\ -\frac{L_\delta}{2}\sin 3\theta_{\mathrm{e}} & \frac{L_\delta}{2}\cos 3\theta_{\mathrm{e}} - L_{\mathrm{s}} & 0 \\ \frac{L_\delta}{2} & 0 & L_{\mathrm{s}} \end{bmatrix} \begin{bmatrix} \frac{\mathrm{d}i_{\mathrm{d}}}{\mathrm{d}t} \\ \frac{\mathrm{d}i_{\mathrm{q}}}{\mathrm{d}t} \\ \frac{\mathrm{d}i_0}{\mathrm{d}t} \end{bmatrix} + \omega_{\mathrm{e}} \begin{bmatrix} -L_\delta \sin 3\theta_{\mathrm{e}} & -L_\delta \cos 3\theta_{\mathrm{e}} - L_{\mathrm{s}} & 0 \\ -L_\delta \cos 3\theta_{\mathrm{e}} + L_{\mathrm{s}} & L_\delta \sin 3\theta_{\mathrm{e}} & L_\delta \\ 0 & 0 & 0 \end{bmatrix} \begin{bmatrix} i_{\mathrm{d}} \\ i_{\mathrm{q}} \\ i_0 \end{bmatrix} \tag{2}$$

where ω_{e} and θ_{e} denote the electrical angular velocity and the electrical angle. The terms i_{d}, i_{q}, and i_0 correspond to the currents along the dq0 axes; U_{d}, U_{q}, and U_0 represent the voltage components of the dq0 axis; R_{s} represents the winding resistance; while L_{s} and L_δ represent the static component and the variable component of the stator inductance.

Assuming ψ_{d} and ψ_{q}, the flux linkages of the d–q axis are represented by Equation (3).

$$\begin{cases} \psi_{\mathrm{d}} = L_{\mathrm{s}} i_{\mathrm{d}} + L_\delta i_0 \\ \psi_{\mathrm{q}} = -L_{\mathrm{s}} i_{\mathrm{q}} \end{cases} \tag{3}$$

The equation for torque in a magnetically linear machine can be derived based on the principle of energy conversion, using an equivalent circuit model that includes elements such as resistance, inductance, and electromotive force (EMF) [14]. For VFRMs, the expression for the instantaneous electromagnetic torque can be described as

$$T_e = \frac{3}{2} N_{\mathrm{r}} \left(\psi_{\mathrm{d}} i_{\mathrm{q}} - \psi_{\mathrm{q}} i_{\mathrm{d}}\right) + \frac{3}{8} N_{\mathrm{r}} L_\delta \left(i_d^2 + i_q^2\right) \sin(3\theta_e + 2\beta) \tag{4}$$

where N_{r} denotes the number of pole pairs in the rotor, and β is the advanced current angle.

According to Equation (4), the instantaneous torque in a VFRM comprises both an average torque and a third-order harmonic torque; the torque ripple arises from the harmonic torque component, directly related to the stator currents' squared values, fluctuating with the third harmonic of the electrical angle. To diminish the torque ripple, it is advantageous to inject the third harmonic currents that contract the original torque ripple. The presence of the term $\sin(3\theta_{\mathrm{e}})$ that the ripple in torque follows a pattern of triple the fundamental electrical frequency. Injecting these harmonic current components effectively attenuates the ripple and enhances motor performance.

With i_{d} not contributing to the average torque, the maximum torque per ampere (MTPA) control approach is adopted for the VFRM to reduce copper losses during operation [15]; this involves setting i_{d} to zero and adjusting i_0 to be equal $1/\sqrt{2} i_{\mathrm{q}}$. In this setup, i_0 corresponds to the amplitude of the DC part of the phase current ($i_{\mathrm{dc}} = i_0$), and i_{q} denotes the magnitude of the AC part ($i_{\mathrm{ac}} = \sqrt{2} i_{\mathrm{q}}$).

3. Harmonic-Injection-Based SSRFT

3.1. VFRM Harmonic Model

In Equation (2), the voltage equations in steady state feature third-order harmonics that are influenced by the self-inductance of the armature windings and correlate with the electrical angular speed. In the dq axis, these third-order harmonic voltages lead to the generation of third-order harmonic currents. Subsequently, the zero axis is affected as per (2), given that it is linked with the d-axis current through the mutual inductance (L_δ). Furthermore, these third-order harmonics can spawn even higher harmonic orders, such as sixth order and beyond, though their amplitudes decrease as the harmonic order increases. According to Equation (4), such harmonic currents generate instantaneous harmonic torques, consequently impacting the accuracy and stability of VFRM negatively.

Following the analysis provided and aiming to minimize torque ripple, the harmonic model was designed for both accuracy and simplicity by focusing solely on the third

harmonic component. This decision is based on the minimal impact of higher-order harmonics on the torque ripple. Voltage Equation (2) is simplified as follows:

$$\begin{cases} u_{\mathrm{d}} = R_{\mathrm{s}} i_{\mathrm{d}} - \omega_{\mathrm{e}} L_{\mathrm{s}} i_{\mathrm{q}} \\ u_{\mathrm{q}} = R_{\mathrm{s}} i_{\mathrm{q}} + \omega_{\mathrm{e}} (L_{\mathrm{s}} i_{\mathrm{d}} + L_{\delta} i_0) \\ u_0 = R_{\mathrm{s}} i_0 \end{cases} \tag{5}$$

Within the synchronous reference frame transformation, the third harmonic voltage vector aligns its rotational direction with that of the fundamental voltage vector, exhibiting a threefold rotational speed denoted by $3\omega_{\mathrm{e}}$. The formulation describing the presence of third-order harmonics in the VFRM's dq0 axis voltage can be described as follows:

$$\begin{cases} u_{dk} = u_{d1} + u_{d3} \cos(3\omega_{\mathrm{e}} t + \theta_2) \\ u_{qk} = u_{q1} + u_{q3} \sin(3\omega_{\mathrm{e}} t + \theta_2) \\ u_{0k} = 0 \end{cases} \tag{6}$$

In the given formula, the variables U_{d1} and U_{q1} represent the components of the fundamental component along the d axis and q axis, respectively. Similarly, U_{d3} and U_{q3} correspond to the third harmonic component in the d–q synchronous rotating coordinate system, along with their initial phase angles, denoted by θ_2. It is important to note that the dq0 voltages become AC components when considering the third harmonic. On the other hand, the value of the zero-sequence voltage is zero in the synchronous rotating coordinate system, as the zero-sequence voltage is orthogonal to U_d and U_q voltages, and its third harmonic could be obtained differently.

The existence of harmonic voltage introduces equivalent harmonic components in the VFRM's three-phase current. The rotation of the third harmonic current aligns with that of the third harmonic voltage in both speed and direction. Upon converting the actual three-phase current of the VFRM into the fundamental component d–q synchronous rotating coordinate system through a coordinate transformation ensuring constant amplitude, the following equations are derived.

$$\begin{cases} i_d = i_{d1} + i_{d3} \cos(3\omega_{\mathrm{e}} t + \theta_3) \\ i_q = i_{q1} + i_{q3} \sin(3\omega_{\mathrm{e}} t + \theta_3) \\ i_0 = 0 \end{cases} \tag{7}$$

Within the equation, i_{d1} and i_{q1} correspond to the fundamental current components along the d axis and q axis, respectively, in the fundamental dq synchronous rotating coordinate system; i_{d3} and i_{q3} represent the amplitude of the third harmonic currents; while θ_3 denotes the initial phase angle of the third harmonic currents.

The steady-state voltage equation for the third harmonic in the coordinate system can be expressed as

$$\begin{cases} {u_{d3}}^* = 3\omega_e L_q i_{q3} + R_s i_{d3} \\ {u_{q3}}^* = -3\omega_e L_d i_{d3} + R_s i_{q3} \end{cases} \tag{8}$$

By integrating Equation (8) into Equation (6), the voltage equation for the fundamental component that includes the third harmonic component is acquired.

$$\begin{cases} u_{dk}^* = -\omega_e L_s i_q + R_s i_{d1} - 3\omega_e L_s i_{q3} \sin(3\omega t + \theta_3) + R_s i_{q3} \cos(3\omega t + \theta_3) \\ u_{qk}^* = \omega_e L_s i_{d1} + R_s i_{q1} + 3\omega_e L_s i_{d3} \cos(3\omega t + \theta_3) + R_s i_{d3} \sin(3\omega t + \theta_3) \end{cases} \tag{9}$$

Given that the harmonic term in (9) represents an AC quantity, the fundamental PI controller, hindered by restricted bandwidth, is unable to eliminate AC errors [16]. Furthermore, the voltages along the dq axis in (5) fail to correct the alternating elements detailed in (9). As a result, the 3rd harmonic current emerges within the dq axis, impacting the VFRM's operation. Consequently, an SSRFT specific to the third harmonic should be established to regulate the d-axis and q-axis currents of the third harmonic.

Based on the abc/dq coordinate transformation principle, the frequency components that rotate at the same speed and in the same direction as the dq synchronous rotating axis system appear as DC components, while the third component is an AC component.

Assuming the fundamental and harmonic currents of the VFRM within the dq rotating coordinate system, the resulting currents on the d–q axis are specified as follows:

$$\begin{cases} i_{dk} = i_{d1} + i'_{d3} \\ i_{qk} = i_{q1} + i'_{q3} \end{cases} \tag{10}$$

where i_{d1} and i_{q1} represent the fundamental currents along the d axis and q axis, respectively; i'_{d3} and i'_{q3} correspond to the assumed third harmonic currents along the d–q axis derived from Equation (7).

Incorporating Equation (10) into the second term of instantaneous torque Equation (4) yields the following expression for the harmonic torque equation:

$$\begin{aligned} T_e &= \tfrac{3}{8} N_r L_\delta \left[(i_{d1}^2 + i_{q1}^2) + (i_{d3}'^2 + i_{q3}'^2 + 2 i_{d1} i'_{d3} + 2 i_{q1} i'_{q3}) \right] \sin(3\theta_e + 2\beta) \\ &= T_{e1} + T_{e3} \end{aligned} \tag{11}$$

where T_{e1} signifies the fundamental electromagnetic torque component, and T_{e3} represents the harmonic component of the electromagnetic torque.

Under the premise of ignoring magnetic saturation, Equation (11) indicates that the fundamental electromagnetic torque arises from the squared magnitudes of the phase currents, proportional to self-inductance variations, and their rate of change relative to rotor position. Meanwhile, the third harmonic component of electromagnetic torque predominantly stems from the interaction between the rotor position, the fundamental current, and the squared magnitude of the third harmonic current. It can also be observed that the torque ripple is directly influenced by the amplitude of the harmonic currents, as well as by the phase relationship between the fundamental and harmonic currents.

3.2. Design of Harmonic Injection Strategy

To mitigate the 3rd harmonic component present in the torque, an equivalent harmonic component is introduced into the reference voltage waveform of the space vector pulse width modulation (SVPWM). This approach aims to neutralize the harmonic content in the current of the VFRM. Based on the analysis conducted, a module is initially developed to extract the third harmonic current from the three-phase current of the VFRM, as depicted in Figure 3.

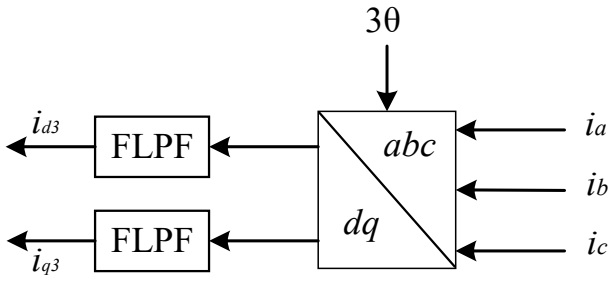

Figure 3. Third harmonic detection.

As the fundamental harmonic current component of a VFRM is a DC component in the corresponding d–q synchronous rotating coordinate axis system, while the other frequency components are AC, it is feasible to achieve the 3rd harmonic current component through a FLPF. A Butterworth filter is the ideal choice as a FLPF due to its ability to provide a frequency response that is maximally flat within the passband, thereby guaranteeing minimal phase distortion and preserving dynamic performance. This characteristic makes

it effective in preventing harmonic current interference without affecting the fundamental frequency components [17]. Its transfer function is

$$TF_f(s) = \frac{\omega_{bw}^2}{(s^2 + \sqrt{2}\omega_{bw}s + \omega_{bw})} \tag{12}$$

In this context, the term ω_{bw} refers to the cutoff frequency of the FLPF. The third-order harmonic of the filtered current feedback signal can be expressed as

$$\left[i_{df3} i_{qf3}\right] = \left[i_{d3} i_{q3}\right] TF_{f3}(s) \tag{13}$$

This process enables the extraction of subharmonic current, resulting in the acquisition of the d-axis and q-axis components (i_{d3} and i_{q3}) of the 3rd harmonic currents within the corresponding synchronous rotating coordinate axis system.

A schematic representation of the third harmonic injection within synchronous rotating coordinates is delineated in Figure 4. In Equation (8), the mitigation of the right terms (resistance voltage drops) is facilitated through fee mechanisms. Through the detection of the 3rd harmonic currents i_{d3} and i_{q3}, the d-axis output voltage that corresponds to the left term in (8) is generated by the PI controller, subsequently integrating it with the q-axis reference voltage U_{q3}*. Conversely, the q-axis PI controller is responsible for deriving an output voltage equivalent to the right side of Equation (8), which is then incorporated into the d-axis reference voltage U_{d3}*.

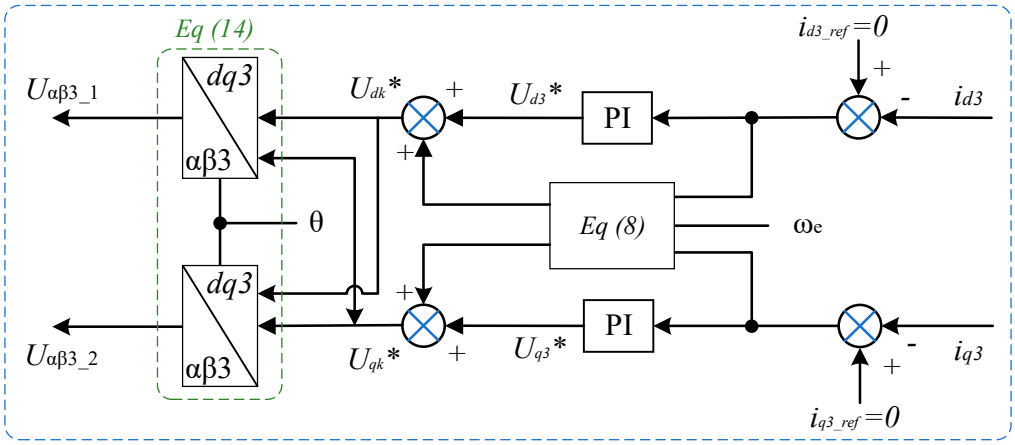

Figure 4. Schematic of the third harmonic injection.

In the absence of implementing the harmonic injection strategy, U_{d3}* and U_{q3}* prove to be inadequate for offsetting the left terms (voltage drop) in Equation (9). Comparatively, the resistance voltage drops, in contrast to the inductance voltage drop, exhibit a relatively minor impact. Notably, U_{d3}* and U_{q3}* do not equate to zero, resulting in the generation of 3rd harmonic currents i_{d3} and i_{q3}. Essentially, the manipulation of the d-axis control voltage U_{d3}* predominantly influences the q-axis harmonic current i_{q3}, while the q-axis control voltage U_{q3}* governs the d-axis harmonic current i_{d3}. It is imperative to acknowledge that the cross-coupling effect of the rotational back-EMF components becomes significantly pronounced at elevated speeds, thus underscoring its importance in the design of the current harmonic regulator.

The resultant U_{dk}* and U_{qk}* are also not inadequate for torque ripple suppression and may induce phase imbalance or overvoltage due to the inductance nonlinearity inherited in the fundamental voltage U_q axis (5) and not included in third harmonic voltage U_{q3}. The negligible zero sequence voltage in the harmonic model can also enlarge the torque ripple and cause current imbalance instead of reducing it, since it contributes to the switching on time of both inverters. When the third harmonic is injected in the U_d axis and U_q axis, the

harmonic voltage interference cannot be prevented; therefore, the performance of VFRM will not be stable.

To avoid the aforementioned problem and ensure a clean harmonic injection and optimal torque ripple reduction, the third harmonic U_{dqk}* voltage needs to be adjusted to incorporate the third-order harmonic of the zero-sequence voltage using (14).

$$\begin{cases} U_{\alpha\beta3\_1} = \frac{\sqrt{3}}{3}U_{dq3}\sin(3\theta_e + \frac{\pi}{3}) - \frac{\sqrt{3}}{3}iU_{dq3}\cos(3\theta_e + \frac{\pi}{3}) \\ U_{\alpha\beta3\_2} = -\frac{\sqrt{3}}{3}iU_{dq3}\sin(3\theta_e + \frac{\pi}{6}) - \frac{\sqrt{3}}{3}U_{dq3}\cos(3\theta_e + \frac{\pi}{6}) \end{cases} \quad (14)$$

By maintaining a 120° phase disparity among open-winding configurations using dual inverters, the third-order harmonic of the U_{dk}* and U_{qk}* voltages undergo a 120○ multiplication, as depicted in Figure 5, resulting in 360°, thus eliminating the generation of any additional third-order harmonic component in the zero-sequence voltage. Consequently, a precise injection of the third harmonic is achieved to suppress torque ripple.

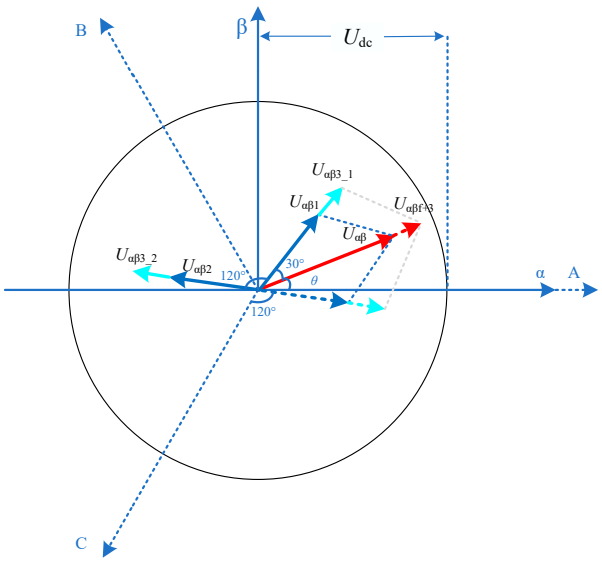

Figure 5. Fundamental voltage reference and resultant third harmonic voltage.

Figure 6 presents a schematic for an overarching control strategy designed to minimize torque ripple by mitigating the harmonics. The structure includes one loop for speed control and three loops for current control. To maximize torque output with the least amount of copper loss, we adopted MTPA control. Additionally, the regulation of counteracting zero-sequence voltage is handled through the adjustment of the zero-sequence current, while the open-winding configuration allows for the passage of the zero-sequence current.

The detection of DC and harmonic elements is performed using a FLPF, followed by their regulation via PI controllers involving phase shifting. The result of the harmonic suppression combines the reference voltages with compensatory harmonic voltages, allowing for the simultaneous regulation of both fundamental and harmonic currents along the dq0 axis.

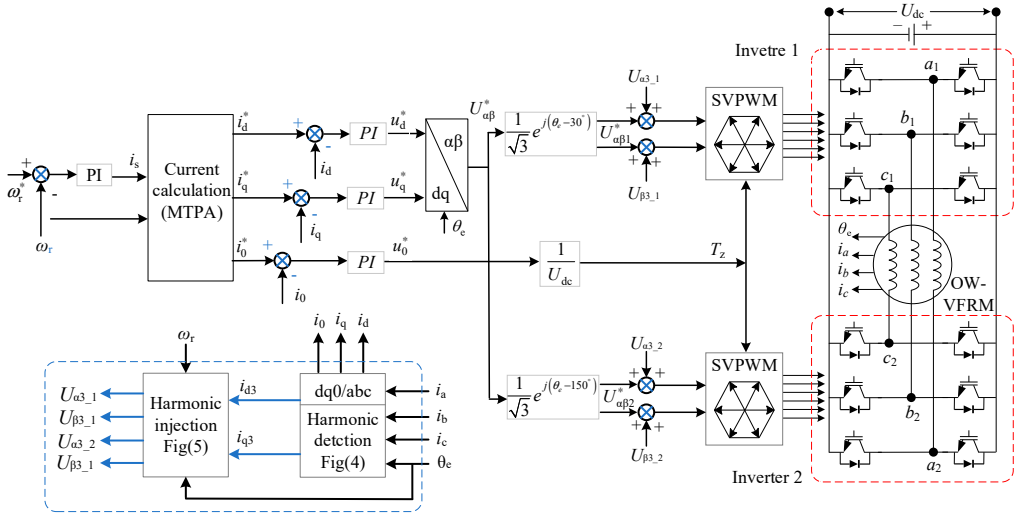

Figure 6. Overall harmonic-injection-based SSRFT strategy.

4. Experimental Results

To validate the harmonic injection strategy-based torque ripple suppression method, an open-winding inverter was established for a 6/4 VFRM. The experimental setup included the parameters of the VFRM employed in this study, as specified in Table 1, while the experimental platform is visually illustrated in Figure 7. Control over the VFRM was conducted by the dual-inverter system, which was regulated by a dSPACE 1202 (dSPACE, Shanghai, China) linked to MATLAB 2015a software, with the IGBT switching frequency set to 10 kHz. Through a Kistler 4502A torque sensor (Kistler, Shanghai, China), the output torque of the VFRM was determined, with the Yokogawa DL850E (Yokogawa, Shanghai, China as the scope.

Table 1. Parameters of the 6/4 VFRM.

Parameter	Value and Unit	Parameter	Value and Unit
Stator outer diameter	90 mm	Number of phases	3
Rotor outer diameter	46.4 mm	Rated torque	0.4
Axial length	25 mm	Poles of stator	6
Air gap	0.5 mm	Phase resistance	3 Ω
Turns per phase	366	AC component of stator inductance (L_s)	30 mH
Current density	5.8 A/mm^2	DC component of stator inductance (L_δ)	24 mH
DC-link voltage (U_{dc})	65 V	Maximum current (i_{max})	2 A

Figure 8a,b show the extracted third harmonic currents and the resultant harmonic voltages for each inverter, experimentally derived using a harmonic detection technique that relies on the three-phase current of the VFRM, specifically when field-oriented control (FOC) is exclusively implemented. It is important to mention that harmonic detection employs only FLPFs, ensuring that the system maintains satisfactory performance. Additionally, these identified currents will undergo further adjustment to minimize torque ripple and enhance voltage utilization.

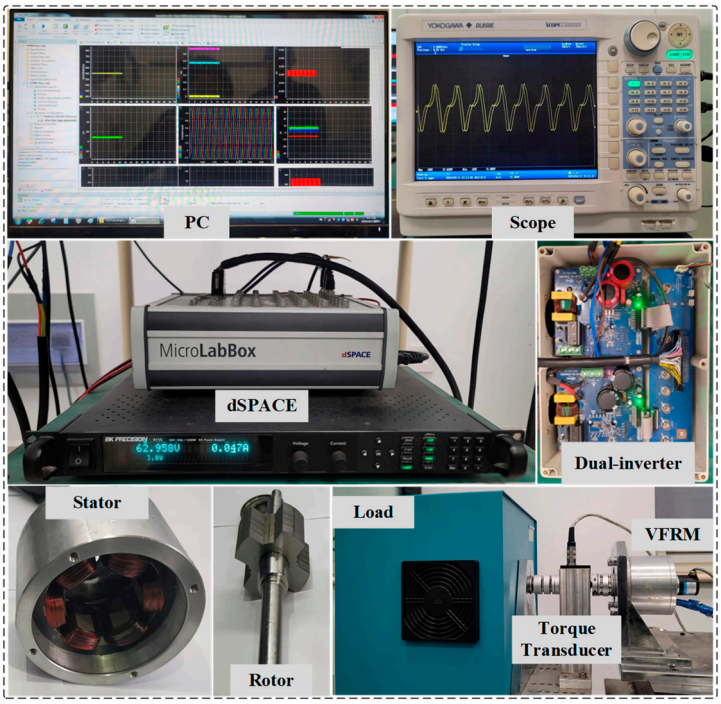

Figure 7. Experimental test rig.

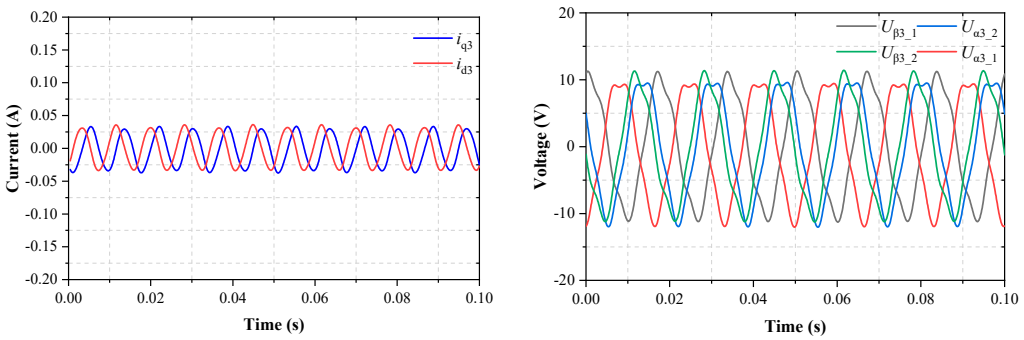

(**a**) (**b**)

Figure 8. (**a**) Extracted harmonics, (**b**) resultant voltages.

The results of experiments at 900 rpm with and without harmonic injection are depicted, presenting the waveforms of electromagnetic torque, three-phase currents, dq-axis currents, and the amplitudes of the reference voltage. The output torque of the VFRM under load conditions with and without harmonic injection is illustrated in Figure 9a,b, indicating a noticeable impact of the harmonic injection on reducing torque ripple, as determined by ΔT_{ripple}, representing the rate of minimized torque ripple. From the figure, it is evident that the torque ripple decreases from 63% to 36%.

$$\Delta T_{ripple} = \frac{T_{e\_\max} - T_{e\_\min}}{T_{avg}} \tag{15}$$

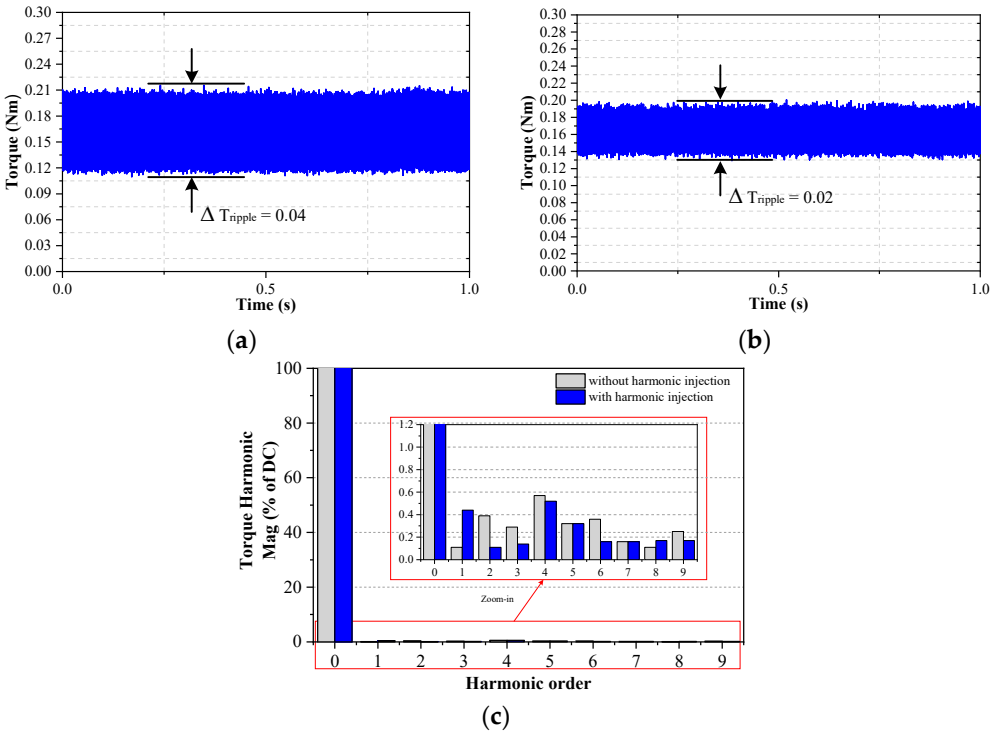

Figure 9. Measured torque of VFRM. (**a**) Without harmonic injection, (**b**) With harmonic injection, (**c**) Comparison of torque harmonic order.

Figure 9c demonstrates the harmonic components of the measured torque acquired from the torque transducer, highlighting the dominance of odd harmonics in the VFRM's torque. As illustrated in Figure 9c (grey bars), the electromagnetic torque exhibits distinct harmonics when the harmonic injection strategy is not implemented on the VFRM. Through fast Fourier transform (FFT) analysis, it is revealed that the 3rd, 5th,6th, and 7th torque harmonics contribute 0.29%, 0.32%, 0.36% and 0.16% of the DC component respectively, with a total harmonic distortion (THD) of 24.67%.

Figure 9c (blue bars) presents the experimental outcomes utilizing the harmonic injection method, where the third, fifth, sixth, and seventh torque harmonics represent 0.14%, 0.32%, 0.16%, and 0.16% of the DC component, while the THD represents 13.48%. Although only the third harmonic is injected to mitigate the torque ripple in the harmonic injection method, it effectively suppresses harmonics, especially the third and sixth. A slight increase in the first harmonic is observed, which is regarded as enhancements in the system performance and torque generation.

Figure 10a,b present the currents in the dq0 axis and the speed; although the level of i_0 and i_d are a little bit higher due to the injection of the third harmonic, there is no notable difference in their variation or stability, indicating that the components of the currents are largely robust to the effects of harmonic injection. On the other hand, the amplitude of i_q current is fairly increased and does not demonstrate a significant difference when the third harmonic is not injected, which implies that third harmonic injection has a bit of an impact on the q-axis current and does not cause any divergence in the system. The most apparent difference is in the motor speed: the motor speed exhibits less fluctuation and appears smoother with harmonic injection, indicating enhanced performance. The reduction in speed ripple points to effective torque ripple suppression, leading to improved motor operation consistency, potentially increased efficiency, and reduced mechanical stress.

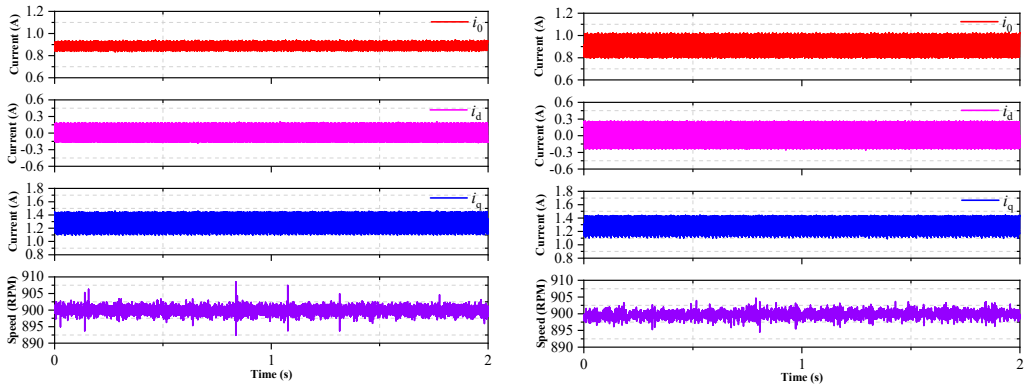

Figure 10. Experimental current comparison: (**a**) without harmonic injection, (**b**) with harmonic injection.

The experimental results corresponding to the original state and harmonic injection method are shown in Figure 11a,b to demonstrate the effects of applying harmonic injection to a VFRM. The three-phase currents are sinusoidal and appear to be balanced, and their peak–peak value is decreased and refined when the third harmonic is injected; this implies the less current used, the more copper loss decreases in the stator phase winding. The reference voltages show some distortion with a much larger amplitude and refined shape when the harmonic injection method is enabled, which indicates the best DC-link utilization.

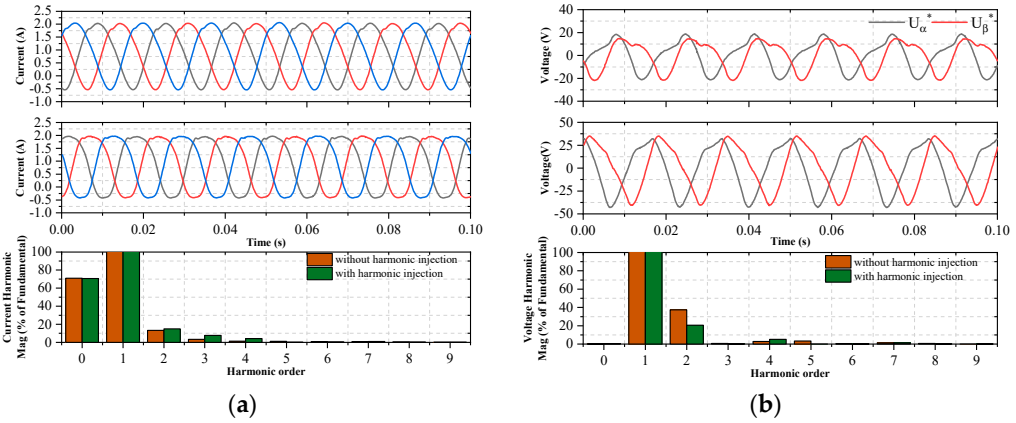

Figure 11. (**a**) Experimental results of three-phase currents: (upside left) without harmonic injection, (middle side left) with harmonic injection, (downside left) comparison of current harmonic order; (**b**) experimental results of reference voltages: (upside right) without harmonic injection, (middle side right) with harmonic injection, (downside right) comparison of voltage harmonic order.

The FFT analysis indicates that without the application of harmonic injection, the significance of the third harmonic in the currents is minimal. Conversely, the implementation of the harmonic injection strategy amplifies the magnitude of the third harmonic, which implies its effectiveness in enhancing electromagnetic torque generation, suppressing higher-order harmonics and reducing torque ripples within VFRM.

In the absence of harmonic injection, the FFT analysis shows that the second, third, fourth, and fifth voltage harmonics contribute 37.41%, 0.65%, 2.93%, and 3.42% to the fundamental component. In contrast, with harmonic injection, the second, third, fourth, and fifth voltage harmonics contribute 20.65%, 0.29%, 5.24%, and 0.12%, respectively, to the fundamental component. This demonstrates that the application of harmonic injection results in a notable reduction in voltage harmonics, particularly for the second and third harmonics. These harmonics are typically the most problematic in VFRMs due to their relationship with the generation of electromagnetic torque and its ripple.

5. Conclusions

This paper presented a harmonic injection method of suppressing torque ripple and enhance the performance of a 6/4 VFRM with open windings. The odd harmonic currents caused by the induced voltage lead to torque ripple and impact the operation stability of VFRMs. According to the harmonic analysis of the mathematical model of a VFRM, the third harmonics can be detected and extracted using FLPF in SSRFT. Then, the third dq-axis currents are controlled and decoupled to obtain accurate compensation voltages, which are then shifted, separated, and included in the reference voltages of each inverter to suppress the torque ripple generated from the VFRM.

The experimental results demonstrate that the harmonic injection method significantly reduces the third harmonic content in the torque, leading to a notable decrease in torque fluctuation. Compared to a VFRM drive without harmonic injection, the proposed method produces a reduction in torque ripple by approximately 50%, validating the effectiveness of the approach. The proposed method is more straightforward to employ, offers enhanced effectiveness in mitigating harmonics, and exhibits a swifter adaptability to dynamic conditions.

Author Contributions: Conceptualization, X.L., E.M.A., A.A. and Y.C.; methodology, X.L. and E.M.A.; software, E.M.A.; validation, X.L. and E.M.A.; formal analysis, X.L. and A.A.; investigation, E.M.A.; resources, X.L., A.A., Y.C. and M.E.A.; data curation, E.M.A. and Y.C.; writing—original draft, E.M.A.; writing—review and editing, X.L., E.M.A., A.A. and Y.C.; visualization, X.L., E.M.A. and Y.C.; supervision, X.L.; funding acquisition, X.L. All authors have read and agreed to the published version of the manuscript.

Funding: Natural Science Foundation of China under Grant 52077055; Projects of Central Government to Guide Local Scientific and Technological Development under Grant 226Z1601G; Tianjin Science and Technology Projects: 22JCZDJC00950.

Data Availability Statement: The original contributions presented in the study are included in the article, further inquiries can be directed to the corresponding authors.

Conflicts of Interest: The authors declare no conflict of interest.

References

1. Liu, X.; Zhu, Z.Q. Comparative study of novel variable flux reluctance machines with doubly fed doubly salient machines. *IEEE Trans. Magn.* **2013**, *49*, 3838–3841. [CrossRef]
2. Liu, X.; Zhu, Z.Q. Electromagnetic performance of novel variable flux reluctance machines with dc-field coil in stator. *IEEE Trans. Magn.* **2012**, *49*, 3020–3028. [CrossRef]
3. Fukami, T.; Matsuura, Y.; Shima, K.; Momiyama, M.; Kawamura, M. A multipole synchronous machine with nonoverlapping concentrated armature and field windings on the stator. *IEEE Trans. Ind. Electron.* **2011**, *59*, 2583–2591. [CrossRef]
4. Hu, W.; Ruan, C.; Nian, H.; Sun, D. Simplified modulation scheme for open-end winding PMSM system with common DC link under open phase fault based on circulating current suppression. *IEEE Trans. Power Electron.* **2020**, *35*, 10–14. [CrossRef]
5. Baiju, M.; Mohapatra, K.; Kanchan, R.; Gopakumar, K. A dual two-level inverter scheme with common mode voltage elimination for an induction motor drive. *IEEE Trans. Power Electron.* **2004**, *19*, 794–805. [CrossRef]
6. Huang, L.R.; Feng, J.H.; Guo, S.Y.; Li, Y.F.; Shi, J.X.; Zhu, Z.Q.; Huang, L.R.; Feng, J.H.; Guo, S.Y.; Li, Y.F.; et al. Rotor shaping method for torque ripple mitigation in variable flux reluctance machines. *IEEE Trans. Energy Convers.* **2018**, *33*, 1579–1589. [CrossRef]
7. Lee, B.; Zhu, Z.Q.; Huang, L.R. Torque ripple reduction for 6-stator/4-rotor-pole variable flux reluctance machines by using harmonic field current injection. In Proceedings of the 2016 IEEE Energy Conversion Congress and Exposition (ECCE), Milwaukee, WI, USA, 18–22 September 2016.
8. Lai, C.; Feng, G.; Iyer, K.; Mukherjee, K.; Kar, N. Genetic algorithm based current optimization for torque ripple reduction of interior PMSMs. *IEEE Trans. Ind. Appl.* **2017**, *53*, 4493–4503. [CrossRef]
9. Flieller, D.; Nguyen, N.; Wira, P.; Sturtzer, G.; Abdeslam, D.; Merckle, J. A self-learning solution for torque ripple reduction for non-sinusoidal permanent magnet motor drives based on artificial neural networks. *IEEE Trans. Ind. Electron.* **2014**, *61*, 655–666. [CrossRef]
10. Chapman, P.; Sudhoff, S.; Whitcomb, C. Optimal current control strategies for surface-mounted permanent-magnet synchronous machine drives. *IEEE Trans. Energy Convers.* **1999**, *14*, 1043–1050. [CrossRef] [PubMed]
11. Beccue, P.; Neely, J.; Pekarek, S.; Stutts, D. Measurement and control of torque ripple-induced frame torsional vibration in a surface mount permanent magnet machine. *IEEE Trans. Power Electron.* **2005**, *20*, 182–191. [CrossRef]

12. Chapman, P.L.; Sudhoff, S.D. A multiple reference frame synchronous estimator/regulator. *IEEE Trans. Energy Convers.* **2000**, *15*, 197–202. [CrossRef] [PubMed]
13. Liu, G.; Chen, B.; Wang, K.; Song, X. Selective Current Harmonic Suppression for High-Speed PMSM Based on High-Precision Harmonic Detection Method. *IEEE Trans. Ind. Inform.* **2019**, *15*, 3457–3468. [CrossRef]
14. Zhu, Z.Q.; Lee, B.; Liu, X. Integrated field and armature current control strategy for variable flux reluctance machine using open winding. *IEEE Trans. Ind. Appl.* **2016**, *52*, 1519–1529.
15. Nakao, N.; Akatsu, K. Suppressing pulsating torques: Torque ripple control for synchronous motors. *IEEE Ind. Appl. Mag.* **2014**, *20*, 33–44. [CrossRef]
16. Nian, H.; Song, Y. Optimized parameter design of proportional integral and resonant current regulator for doubly fed induction generator during grid voltage distortion. *IET Renew. Power Gen.* **2014**, *8*, 299–313. [CrossRef]
17. Nako, J.; Psychalinos, C.; Elwakil, A.S. A 1+ α order generalized Butterworth filter structure and its field programmable analog array implementation. *Electronics* **2023**, *12*, 1225. [CrossRef]